Journal of Sound and Vibration (2001) **239**(1), 69–97
doi:10.1006/jsvi.2000.3157, available online at http://www.idealibrary.com on IDEAL®

VIBRATION ANALYSIS OF RAILWAY TRACK WITH MULTIPLE WHEELS ON THE RAIL

T. X. WU†

State Key Laboratory of Vibration, Shock and Noise, Shanghai Jiao Tong University, Shanghai 200030, *P.R. China*

AND

D. J. THOMPSON

*Institute of Sound and Vibration Research, University of Southampton, Southampton SO*17 1*BJ, England*

(*Received* 1 *June* 1999, *and in final form* 30 *May* 2000)

The major source of railway rolling noise is the structural vibration of the wheel and rail which is generated by the combination of small-scale undulations (roughnesses) on the wheel and rail contact surfaces. Usually, the rail vibration behaviour is studied using a model in which only a single wheel is present. This is not the case in practice, where multiple wheels roll on the rail. It is shown first that the high-frequency excitation from each wheel can be treated independently by using the superposition principle, provided that the rail vibration is considered as a frequency band average. The appropriate application of the superposition principle is then to model the rail vibration as a sum of cases in which all wheels are retained in contact with the rail but the roughness at all but one of them is set to zero. The presence of multiple wheels on the rail leads to reflections of waves in the rail. The paper explores such effects on the rail vibration caused by multiple wheels acting as supplementary dynamic systems. The receptance of a rail with a single additional wheel on it is studied first to acquire a physical insight into the effects of wheels on the rail vibration. Then more complicated models are developed and used to investigate the effects of multiple wheels on a rail. Practical consequences due to the multiple wheel–rail interactions are also presented.

1. INTRODUCTION

The source of railway rolling noise is the structural vibration of the wheel and rail which is generated by the combination of small-scale undulations (roughnesses) on the wheel and rail contact surfaces. When a train runs along the track, these roughnesses produce dynamic interaction forces between the wheel and rail at the frequencies corresponding to the passage speed over the particular roughness wavelength. These forces cause the wheel and rail to vibrate and radiate noise. Some simple relative displacement (roughness) excitation models in the frequency domain were proposed by Remington [1] and Grassie *et al.* [2], giving the complex amplitude of the contact force F as

$$F = -\frac{r}{(\alpha^W + \alpha^C + \alpha^R)}, \tag{1}$$

† Currently at ISVR, University of Southampton, U.K.

0022-460X/01/010069 + 29 $35.00/0

where r is the relative displacement (roughness) between the wheel and rail and α^W, α^C and α^R are the point receptances (displacement divided by force) of the wheel, contact spring and rail respectively at each frequency. A more comprehensive model was developed by Thompson [3] which can be used for calculating the wheel–rail dynamic interaction forces in up to six degrees of freedom.

Knothe and Grassie [4] presented a review of different models for wheel–rail interaction and for track vibration. The former were divided into a stationary load, a moving load, a moving irregularity between a stationary wheel and the rail (as in the equation (1) above) and a wheel rolling over irregularities on the track. Since the wave speeds in the rail corresponding to audio frequencies are much higher than the train speed it does not cause problems to simplify the wheel–rail interaction model by regarding the train as stationary, i.e. using the moving irregularity model.

When the point receptances of both the wheel and the rail are known, the wheel–rail interaction force, and thus the vibration level of the wheel and rail, can be estimated according to their combined roughness spectrum, by using equation (1). The point receptances are thus an essential element of the model.

Different models have been developed over the years [4] to investigate the dynamic behaviour of the rail. Simple beam models were used by Grassie *et al.* [2] and Heckl [5]. More advanced models based on the finite element method were used by Thompson [6], Ripke and Knothe [7] and Gry [8] to calculate rail receptances for either vertical or lateral vibration at high frequencies. Recently, a double-beam model and a multiple beam model of a rail have been developed by Wu and Thompson [9, 10] to analyze the vertical and lateral vibration properties respectively. Some other factors such as random sleeper spacing and non-linear properties of the pad and ballast also affect the vibration behaviour of the railway track. These effects have been studied by Heckl [11] and Wu and Thompson [12].

In all the references cited above, whether by using FE models or a single- or multiple-beam model, the rail vibration behaviour is studied by using a model in which the wheel–rail interaction is not considered, apart from at the single wheel–rail contact at which excitation takes place. Thus, the physical system is replaced by one in which only a single wheel is coupled to the rail. The dynamic interaction force between the wheel and rail may then be determined by using the relative displacement excitation (moving irregularity) models [1–3]. These require the point receptances of the wheel and rail when not in contact with each other, as in equation (1). Obviously, in practice, multiple wheels are present on the rail, but treating the response to a single wheel provides a useful simplification. It is then assumed in these models that the average response of the rail to multiple wheels can be obtained by combining the mean-square responses to a series of single wheels.

Thompson [13] carried out some simple analysis of the effects of an additional wheel on a rail, but it is very limited. Igeland [14], using a moving vehicle model, considered a two-wheel bogie on a single rail and found some evidence of standing wave effects. Also multiple wheels are considered in multibody models of vehicles but these are used at low frequencies only, without any interaction through the track.

There are two issues to be addressed in considering the effects of multiple wheels on a rail. The first is how to combine the track response induced by the excitation due to each wheel by using the principle of superposition. It has usually been assumed that the mean-square responses due to each wheel can be added: i.e., that the inputs from each wheel can be treated as uncorrelated with one another. A treatment in which the excitations at each wheel are regarded as strictly correlated is not appropriate in the general case, as the roughness inputs are in part due to those on the individual wheels, which are unrelated. The validity of taking the excitations to be wholly uncorrelated is considered in section 2, where it is shown that it gives acceptable results provided that (i) a sufficiently wide frequency

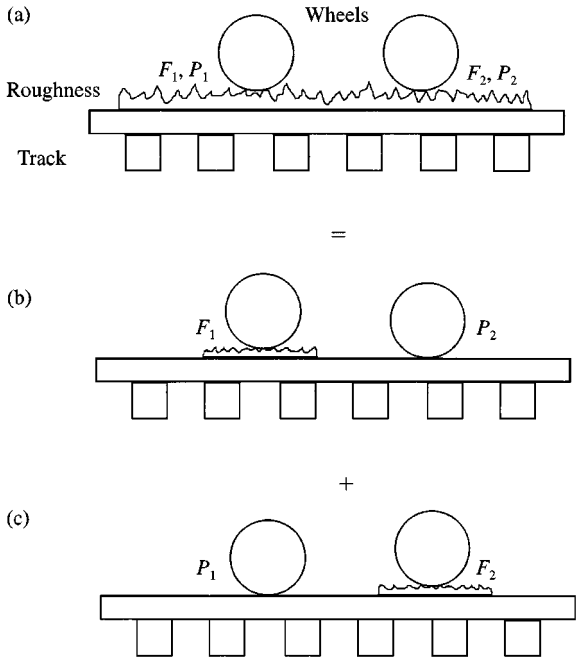

Figure 1. Superposition procedure of the track response to two wheel–rail interactions.

band average is studied, typically a bandwidth of at least 20 Hz, (ii) the decay of vibration in the track is sufficiently large or (iii) the dominant roughness is present on the wheel.

After having shown that the excitation at each wheel can be treated as uncorrelated, the principle of superposition is used to separate the response caused by each independent excitation. The excitation due to the roughness acting at each wheel has the form of a relative displacement, and it is these relative displacements rather than the interaction forces which are independent. As shown in Appendix A and indicated in Figure 1, a track excited by two wheels can be notionally replaced by one with wheel 1 'active' (with roughness excitation) and wheel 2 'passive' (with roughness set to zero) and another with wheel 2 active and wheel 1 passive. This approach can be extended to situations with multiple wheels, where the basic case to be studied is the response of the track to excitation at a single wheel, with the remaining wheels acting as passive dynamic systems coupled to the rail. In the remainder of the paper, models for this are developed, starting with a rail coupled to a single additional wheel and then considering more complex systems of multiple wheels.

Assuming one wheel to be active and the remaining wheels to be passive is thus an intermediate step to obtaining the response of the track to the roughness under one wheel. The response due to roughness under all wheels is then obtained by superposition.

The main purpose intended for the models developed here is to predict the noise from the track. This can be estimated from the integral of the squared vibration amplitude over a length of track along with the sound radiation properties of the rail or sleepers. Although the noise is usually presented in frequency bands such as one-third octaves, results are given here in narrow frequency steps in order to clarify the phenomena observed.

Throughout this paper linear models for the vibration are assumed to be valid. The models are only developed for vibration in the vertical direction, although in a similar way, the effects of wheel–rail interactions on the lateral vibration can also be studied if an

appropriate rail model is used for lateral vibration, as, for example by Wu and Thompson [10].

2. MULTIPLE WHEEL–RAIL INTERACTIONS

2.1. USING THE SUPERPOSITION PRINCIPLE TO SEPARATE THE TRACK RESPONSE

When a train runs on a track, each wheel interacts with the track. Vibration is induced by the roughnesses on the wheel tread and the rail-head surface at each wheel–rail contact.

The track vibration response to multiple wheel–rail interactions can be simplified by using the superposition principle, since the system is assumed to be linear. To illustrate this, Figure 1 shows a situation with two wheels on a rail. Coupling between the wheels through the vehicle is ignored as the soft suspension springs isolate the wheels from each other at the frequencies of interest here; i.e., above 50 Hz. The combined vibration, see Figure 1(a), is the sum of that induced by the roughness at the first wheel, see Figure 1(b), and that induced by the roughness at the second wheel, see Figure 1(c). It is generally simpler to calculate the vibration for a single input, rather than simultaneously for multiple inputs. The mathematical basis of the approach summarized by Figure 1 is given in Appendix A.

A question which now arises is whether the two inputs in Figure 1(b) and 1(c) are related to one another. If so, the two responses should be added allowing for relative phase; if not, the mean-square responses can simply be added. It should be noted that the roughness excitation at each wheel/rail contact is a combination of wheel and rail roughness. The roughness on each wheel is independent of that on the other, so in the presence of only wheel roughness, the excitation at each wheel should be considered as incoherent. On the other hand, in the case where the roughness is only on the rail, the relative phase of the two excitations should, in principle, be included in this sum. The question of which model is the more appropriate for a combination of wheel and rail roughness will be addressed further in sections 2.2 and 2.3 below.

It should also be noted that, in the two separate cases, shown in Figure 1(b) and 1(c), both wheels are still present on the track. One is now an "active" wheel, at which roughness is present, and the other is a "passive" wheel. At the active wheel an interaction force F_i is induced by the roughness. This may be termed the "original" excitation force. At the passive wheel an interaction force P_j is also present. This is a secondary force, induced by rail vibration produced by the original force F_i. It is correlated with the force F_i, and is proportional to it. The original force, F_i, can be determined by using the relative displacement excitation model, equation (1), but the rail receptance used here should be calculated by using a track model which includes the additional passive wheel, as shown in Appendix A.

In the combined situation, see Figure 1(a), the interaction force at each wheel comprises an active component, due to the roughness at this wheel, and a passive component due to the roughness at the other wheel.

2.2. INTERFERENCE BETWEEN MULTIPLE COHERENT WHEEL–RAIL EXCITATIONS

This section addresses the relationship between the original forces F_1 and F_2 at the two wheels of Figure 1. Suppose, for simplicity, that both wheels are excited by the same roughness on the rail, with a time lag $t_0 = l/v$ corresponding to their spatial separation, l and the train speed v. The forces acting are thus $F(t)$ and $F(t - t_0)$.

The roughness $r(z)$ can be regarded as an ergodic stationary random process. It has components up to wave numbers corresponding to at least 5 kHz. If the broad-band response over the whole audio frequency range is considered, it is found that the forces F_1 and F_2 are uncorrelated: that is, their broad-band correlation coefficient is negligibly small. On the other hand, if a sufficiently narrow frequency band is considered (in the limit this is a sine wave) they are perfectly correlated. The degree of correlation also depends on the time lag t_0. In the limit $t_0 \to 0$, F_1 and F_2 are clearly equal.

In practice, random vibration is usually studied in frequency bands. In Appendix B it is shown that, provided the response is studied in bands with a bandwidth of at least $0{\cdot}8/t_0$, the track response at an arbitrary position deviates by less than 1 dB from that due to two incoherent forces. For a typical case of two wheels in a bogie separated by $l = 1{\cdot}8$ m, and for a train speed, $v = 44$ m/s (160 km/h) this condition corresponds to a minimum bandwidth of 20 Hz, which is satisfied, for example, by one-third octave bands above 80 Hz. For larger spacings between wheels or lower speeds this minimum bandwidth is reduced.

The fact that the vibration of the rail decays strongly with distance at low frequencies also suppresses any interference between the excitation at different wheels. For a decay rate of 10 dB/m, typical of frequencies below 200 Hz [15], the effects of interference between F_1 and F_2 on the track vibration are limited to less than ± 1 dB, irrespective of the bandwidth used.

2.3. DISCUSSION

Since, in practice, the roughness is a combination of that on the wheels and that on the rail, it is clearly convenient to be able to use a single model for their influence. The above analysis has shown that even two wheels running over exactly the same rail roughness can be treated as generating uncorrelated original forces F_1 and F_2, provided that the response is analyzed in suitable frequency bands. This does not provide an unreasonable constraint.

This means that the mean-square response of the track to the excitation caused at each active wheel can be added by using the superposition principle, *without the need to consider the relative phase of these separate responses.* However, for a given active wheel, the passive wheel–rail interactions due to the consequent track vibration, cannot be treated as uncorrelated with each other.

The purpose of the remainder of this paper is to study the effects on the track vibration of the passive wheel–rail interactions. In the following sections, a suitable track model is developed, in which only one wheel actively excites the track, this wheel being replaced by an excitation force, whereas the other wheels are attached to the rail as passive systems. The dynamic behaviour of this track model is very important, because each active wheel–rail excitation force F_i can be determined by using the point receptance from this model in equation (1), and then the response to this excitation can also be calculated by using this track model. Although the need to analyze vibration and noise in frequency bands with a bandwidth of at least 20 Hz should be borne in mind; for clarity in the remainder of the paper, results are given in frequency steps of 10 Hz.

3. RECEPTANCES OF THE UNCOUPLED SYSTEMS

In order to calculate the effects of wheel–rail interactions, the individual receptances of the rail, wheel and contact spring are required in the absence of coupling.

3.1. RECEPTANCES OF A RAIL

In this paper a conventional Timoshenko beam model is employed to calculate the receptances of a rail without a wheel on it. Although a conventional beam model is only reliable below 2000 Hz for the vertical vibration of the rail foot, it can be used for predicting the rail head response for frequencies up to close to the frequency at which the higher order "foot flapping" wave cuts on: i.e., up to about 5000 Hz [9]. At high frequencies the wave propagation decay rate of a conventional beam model falls continuously, whereas in practice the decay rate increases slightly with increasing frequency above about 1–2 kHz [15]. Thus, a small loss factor needs to be assigned to the rail to enhance the decay rate at high frequencies. Details about modelling of a discretely supported rail and calculations of track receptances can be found in reference [9]; here only the results are summarized.

Figure 2 shows the point and transfer receptances of a discretely supported UIC 60 rail with the excitation acting either at mid-span or above a sleeper. The transfer receptances are presented at 0·9, 1·8 and 3·6 m from the excitation point. The parameters for the rail are

$$E = 2{\cdot}1 \times 10^{11}\ \mathrm{N/m^2}, \quad G = 0{\cdot}77 \times 10^{11}\ \mathrm{N/m^2}, \quad \rho = 7850\ \mathrm{kg/m^3}, \quad \eta_r = 0{\cdot}01,$$

$$A = 7{\cdot}69 \times 10^{-3}\ \mathrm{m^2}, \quad I = 30{\cdot}55 \times 10^{-6}\ \mathrm{m^4}, \quad \kappa = 0{\cdot}4,$$

where E is the Young's modulus, G the shear modulus, ρ the density, η_r the loss factor of the rail, A the cross-sectional area, I the area moment of inertia and κ the shear coefficient. The parameters for the discrete support are

$$K_p = 350\ \mathrm{MN/m}, \quad \eta_p = 0{\cdot}25, \quad K_b = 50\ \mathrm{MN/m}, \quad \eta_b = 1{\cdot}0, \quad M_s = 162\ \mathrm{kg}, \quad d = 0{\cdot}6\ \mathrm{m},$$

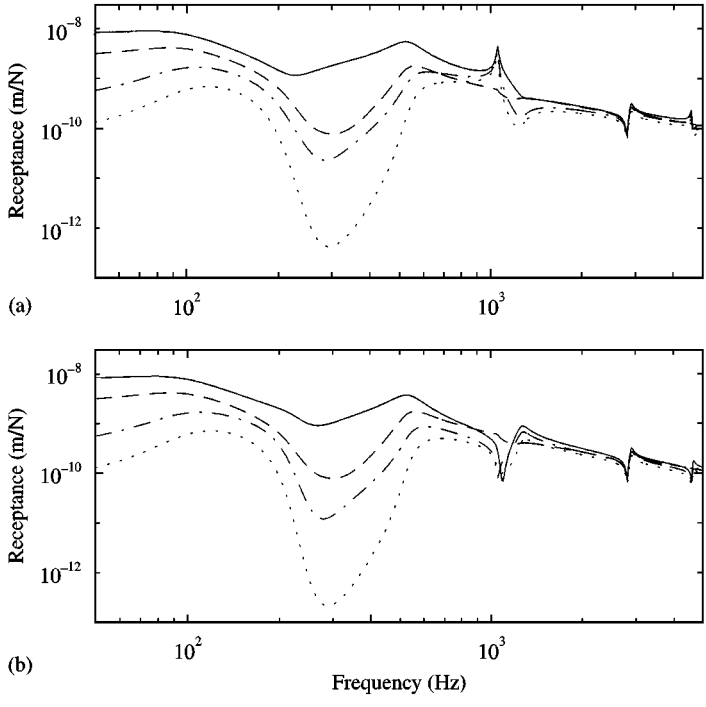

Figure 2. Point and transfer receptances of a discretely supported rail: (a) excitation at mid-span, (b) excitation above a sleeper. —— Point receptance, – – – transfer receptance at 0·9 m, –·–·– transfer receptance at 1·8 m, ····· transfer receptance at 3·6 m.

where K_p is the pad stiffness, η_p the loss factor of the pad, K_b the ballast stiffness, η_b the loss factor of the ballast, M_s the sleeper mass and d the span length. These parameters correspond to a track with concrete sleepers and moderately stiff rail pads. Similar parameters were used by Wu and Thompson [9] and Vincent and Thompson [15] for track C.

The point receptances for the rail can be seen to reach resonances at about 80 and 530 Hz, and there are also three pinned–pinned resonances which appear at about 1050, 2800 and 4600 Hz. For detailed discussion of these resonances, see reference [9]. From Figure 2(b), by comparing the transfer receptances at different positions, it can be seen that the wave propagation decay rate is high in the low-frequency region and low in the high-frequency region. At about 300 Hz the decay rate is the highest. These features are very useful in understanding the results of the later analysis of the effects of the wheel–rail interaction on the rail vibration.

3.2. WHEEL RECEPTANCE

The wheel receptance can be obtained either by finite element analysis or by experiment [16]. Here only the point receptance of a wheel in the radial direction at the contact point with the rail is needed. The radial point receptance of a wheel can be approximated by using the simple model shown in Figure 3. In this model the wheel is composed of a mass M_W (all the unsprung mass) and a modal spring K_M which represents the stiffness of high-frequency modes. The point receptance is

$$\alpha^W = \frac{1}{K_M} - \frac{1}{M_W \omega^2}. \tag{2}$$

From equation (2) the wheel can be seen to vibrate as a mass at low frequency and as a spring at high frequency. The receptance from the simple model is mainly used in this paper, whereas that from an FE model is used only for some comparisons.

Figure 4 shows the wheel receptances from the FE model (including the unsprung mass) and the simple model. The modal stiffness K_M of the simple model is chosen according to the mass M_W to match the main trough of the receptance from the FE model at the corresponding frequency of 430 Hz. The wheel parameters are chosen from a UIC 920 mm standard freight wheel. The unsprung mass is $M_W = 600$ kg which is approximately equal to half the weight of the wheelset.

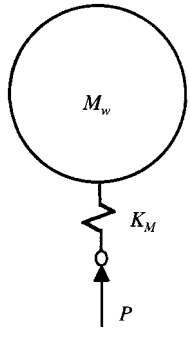

Figure 3. A simple model of the wheel (including unsprung mass).

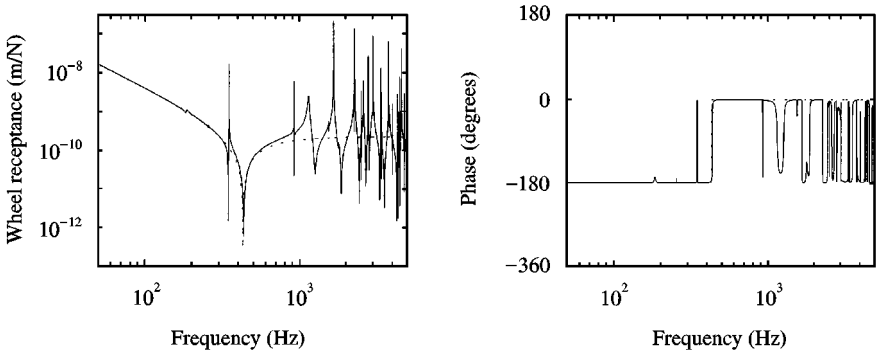

Figure 4. Wheel (including unsprung mass) receptance: —— from the FE model, ····· from the simple model.

It can be seen that there are a number of sharp peaks and troughs for the wheel receptance at high frequencies due to the low damping of the wheel. Since a fairly large tolerance in web thickness is allowed in the wheel manufacturing and differences in diameter occur due to wear, the peaks or troughs in the high-frequency region will occur at different frequencies for each individual wheel. The receptance of the simple model can be seen to be close to the average of the peaks and troughs of the FE model in this high-frequency region.

3.3. CONTACT SPRING

The contact spring between the wheel and the rail is effectively non-linear and follows the Hertz law. However, since the dynamic displacements are small, it is possible to treat the contact spring as a constant linear stiffness K_H. The value of K_H should be determined by using the contact theory of Hertz according to the preload between the wheel and rail and their radii of curvature. Here the contact spring is calculated as in reference [13], giving $K_H = 1{\cdot}14 \times 10^9$ N/m for a 50 kN preload. The contact spring receptance α^C is the inverse of K_H.

3.4. COMBINED RECEPTANCE

From equation (1) it can be seen that the point receptance sum of the wheel, contact spring and rail plays a very important role in determining the wheel–rail dynamic interaction force. Figures 5(a) and 5(b) show the point receptance sum of the wheel (using the simple model), contact spring and discretely supported rail along with the individual receptances for the cases of excitation acting at mid-span or above a sleeper. It can be seen that in both cases in Figures 5(a) and 5(b) the sum of the receptances is similar except near the first pinned–pinned resonance. In the frequency range 100–900 Hz the point receptance sum is high and almost the same as the rail receptance, whereas at high frequencies it becomes very close to the receptance of the contact spring and much higher than the rail receptance. For the excitation acting at mid-span (Figure 5(a)) the point receptance sum can be seen to fall immediately after the first pinned–pinned resonance to a value close to the wheel receptance. The reason for this is that the magnitude of the rail receptance drops after the first pinned–pinned resonance and its phase is close to $-\pi$ so that at a certain frequency, a little above the pinned–pinned resonance the receptances of the rail and the contact spring are equal to each other in magnitude but out of phase, and thus cancel each other.

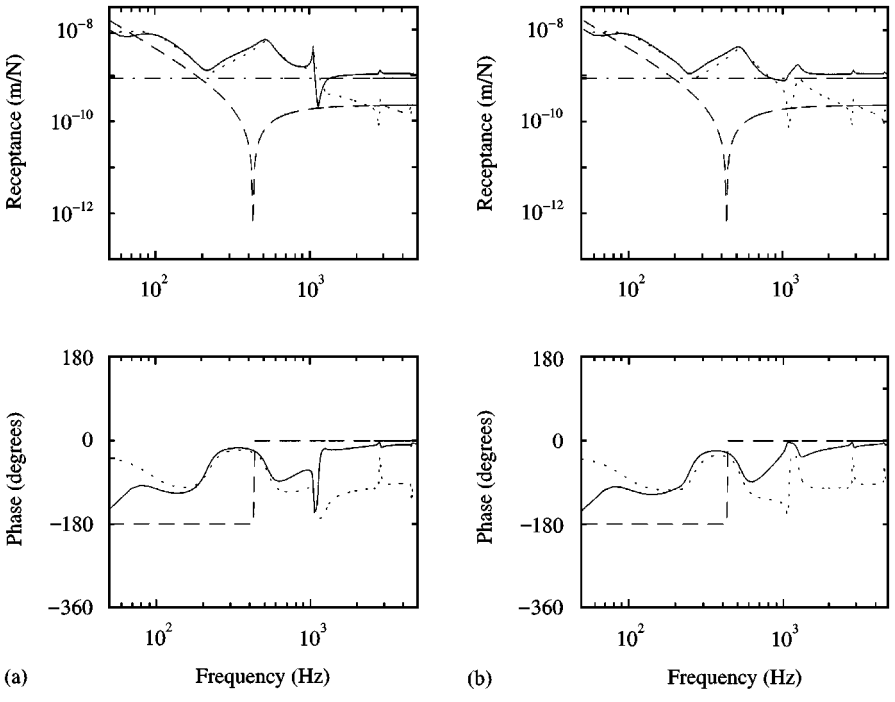

Figure 5. Point receptance sum of the wheel, contact spring and rail: (a) discretely supported rail with excitation at mid-span, (b) discretely supported rail with excitation above a sleeper. —— Point receptance sum, – – – wheel receptance, –·–·– contact spring receptance, ····· rail receptance.

4. RAIL VIBRATION BEHAVIOUR WITH A SINGLE WHEEL ON IT

4.1. MODEL

A vibration model of a rail with only one passive wheel on it is considered first as a simple case to gain insight. When using this model, the receptances of the rail can be determined by means of the receptances of the wheel and the rail without the wheel on it and some most important characteristics of the effects of wheel–rail interaction on the rail vibration can be obtained. For wagons which have only one wheelset at each end, this model can be used directly to obtain a practical solution. This is because, although a train contains many wheelsets running on the rail, the effect of one wheel on the interaction caused by another can be ignored for wheels that are further apart than about 10 m, because the wave decay rate in the rail is usually at least 0·5 dB/m. The distance between the two wheelsets at opposite ends of a wagon is usually greater than 10 m, whereas the two closest wheelsets on adjacent wagons are closer than this.

Consider a rail having a single passive wheel on it at $z = a$ and an external excitation (for example due to another wheel) at $z = 0$, as shown in Figure 6. Here only one direction of vibration of the rail is taken into account, which could be either vertical or lateral, and the cross-interaction of the vertical and lateral vibrations is ignored for simplicity. Coupling with the far rail through the sleepers or axles is also ignored. It is assumed that forces and responses are harmonic and both have an $e^{i\omega t}$ dependence, the $e^{i\omega t}$ term usually being omitted. In Figure 6, F and u_i represent the external force and the incident wave produced by F respectively. The incident wave propagates along the rail and interacts with the wheel at $z = a$. This results in the generation of an interaction force P between the wheel and rail at the contact position. The generated wave produced by P is

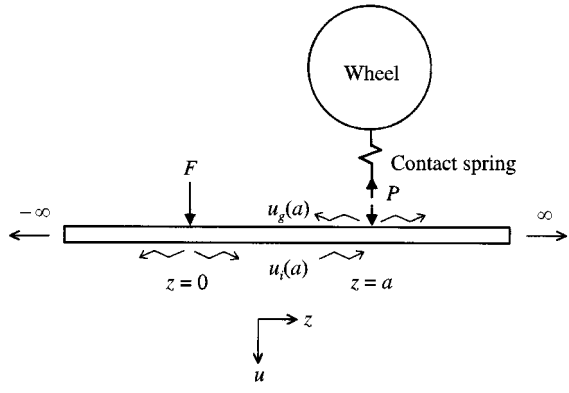

Figure 6. Railway track model with a single wheel on the rail.

represented by u_g. Thus, the vibration of the rail is a combination of the incident wave u_i and the generated wave u_g. The response of the rail at the wheel–rail contact point $z = a$ to the external force F at $z = 0$ is given as

$$u(a) = u_i(a) + u_g(a) = F\alpha_F^{RT}(a) + P\alpha_P^R, \tag{3}$$

where α_F^{RT} and α_P^R are the transfer and point receptances of the rail respectively. Equation (3) can be used with either a continuously supported, or a discretely supported rail. For a discretely supported rail model, since F and P may act at different positions in a span between two sleepers, the receptances corresponding to F and P are generally not the same. Thus, the subscripts F and P are used for marking the corresponding receptances. For a continuously supported rail or a discretely supported rail where both F and P act either at mid-span or above a sleeper, the receptances for F and P are the same and the subscripts need not be used.

If the dynamic stiffness of the wheel, Z_w (including the wheel–rail contact spring stiffness), is known at the frequency ω, the dynamic interaction force P can be represented by

$$P = -Z_w u(a) = -Z_w[u_i(a) + P\alpha_P^R]. \tag{4}$$

Since $1/Z_w = \alpha^W + \alpha^C$, where α^W and α^C represent the receptances of the wheel and contact spring respectively, substituting it into equation (4) gives

$$P = -\frac{u_i(a)}{\alpha^W + \alpha^C + \alpha_P^R} = -\frac{\alpha_F^{RT}(a)}{\alpha^W + \alpha^C + \alpha_P^R} F. \tag{5}$$

The wheel–rail interaction force can be seen from equation (5) to be related to the sum of point receptances of the wheel, contact spring and rail. This term also appears in the expression for roughness excitation; see equation (1). P also depends on the transfer receptance of the rail. If the point receptance of the wheel, contact spring or rail is high or the transfer receptance of the rail is low, the interaction force P will be small. Low transfer receptance occurs when the wave propagation decay rate is high, and thus the rail vibration at $z = a$, caused by the original force F, is weak. As a result, the interaction force P is small.

When the generated interaction force P is known, the vibration displacement of the rail at any point can be obtained by superposing the incident and generated waves:

$$u(z) = F\alpha_F^{RT}(z) + P\alpha_P^{RT}(z-a) = F\left[\alpha_F^{RT}(z) - \frac{\alpha_F^{RT}(a)}{\alpha^W + \alpha^C + \alpha_F^R}\alpha_P^{RT}(z-a)\right]. \tag{6}$$

Thus, the transfer and point receptances of the rail with a single wheel on it are given as

$$\alpha_w^{RT}(z) = \frac{u(z)}{F} = \alpha_F^{RT}(z) - \frac{\alpha_F^{RT}(a)}{\alpha^W + \alpha^C + \alpha_P^R}\,\alpha_P^{RT}(z-a), \tag{7}$$

$$\alpha_W^R = \frac{u(0)}{F} = \alpha_F^R - \frac{[\alpha_F^{RT}(a)]\,[\alpha_P^{RT}(-a)]}{\alpha^W + \alpha^C + \alpha_P^R} = \alpha_F^R - \frac{[\alpha_F^{RT}(a)]^2}{\alpha^W + \alpha^C + \alpha_P^R}, \tag{8}$$

where $\alpha_F^{RT}(a)$ and $\alpha_P^{RT}(-a)$ are equal because of the reciprocity, and the subscript w means the rail having a wheel (or wheels) on it.

From equations (7) and (8) it can be observed that the receptances of the rail with a single wheel on it are determined by the point and transfer receptances of a 'bare' track (without any wheel–rail interaction), the receptance of the wheel and that of the contact spring, which have been derived in section 2.

Results will be presented for a discretely supported rail model. For simplicity both the external excitation and the additional wheel–rail interaction are assumed to act either at mid-span or above a sleeper, i.e. a is an integer multiple of the sleeper spacing. In this case, the subscripts for rail receptances in equations (3)–(8) need not be used.

4.2. SIMPLE ANALYSIS

Before calculating the point and transfer receptances by using equations (7) and (8), it is helpful to carry out some simple analysis in order to get a better understanding of the results. The ratio

$$\frac{\alpha_W^R}{\alpha^R} = 1 - \frac{[\alpha^{RT}(a)]^2}{\alpha^R(\alpha^W + \alpha^C + \alpha^R)} \tag{9}$$

may be used for quantifying the variation of the point receptances of the rail with a single wheel on it compared with the case without the wheel. Because the wave propagation decay rate in a supported rail is high at low frequencies, see Figure 2, the transfer receptance $\alpha^{RT}(a)$ is much smaller than the point receptance α^R when the distance a is large enough, for example greater than 1·8 m. In addition, the receptance sum $\alpha^W + \alpha^C + \alpha^R$ is very close to the point receptance α^R at low frequencies; see Figure 5. As a result, the second term on the right-hand side of equation (9) is close to zero, and thus the following approximation holds at low frequencies:

$$\alpha_w^R/\alpha^R \approx 1. \tag{10}$$

Therefore, *at low frequencies the point receptance of a rail with a single wheel on it may be regarded as approximately equal to that of a rail without a wheel on it.*

At high frequencies the following relationship holds; see Figure 5:

$$|\alpha^W + \alpha^C + \alpha^R| \gg |\alpha^R| > |\alpha^{RT}(a)|. \tag{11}$$

Thus, the magnitude of the second term on the right-hand side of equation (9) is less than unity at high frequencies. In addition, although the distance a is constant, the phase of the second term continuously changes from $-\pi$ to π as the vibration frequency increases from low to high. This is because the wave number undergoes a continuous increase with increasing frequency and thus the phase of $\alpha^{RT}(a)$ continuously changes from $-\pi$ to π. Therefore, it is expected that *at high frequencies the point receptance of the rail with a single*

wheel on it will fluctuate around the point receptance of the rail without a wheel on it. Moreover, *this fluctuation becomes smaller and smaller with increasing frequency* because the ratio of the rail receptance α^R (or $\alpha^{RT}(a)$) to the receptance sum $\alpha^W + \alpha^C + \alpha^R$ becomes smaller and smaller (see Figure 5).

Similarly, for the transfer receptance, the ratio

$$\frac{\alpha_w^{RT}(z)}{\alpha^{RT}(z)} = 1 - \frac{\alpha^{RT}(a)}{\alpha^W + \alpha^C + \alpha^R} \frac{\alpha^{RT}(z-a)}{\alpha^{RT}(z)} \tag{12}$$

can be used to examine the variation of the transfer receptance of a rail with a single wheel on it compared with the case without the wheel. However, situations are more complicated in terms of transfer receptance compared with the point receptance because both frequency and spatial position affect the transfer receptance. For example, when $z = a/2$, a, $2a$ and $-a$, the ratios are given as follows:

$$\frac{\alpha_w^{RT}(a/2)}{\alpha^{RT}(a/2)} = 1 - \frac{\alpha^{RT}(a)}{\alpha^W + \alpha^C + \alpha^R}, \quad z = a/2, \tag{13a}$$

$$\frac{\alpha_w^{RT}(a)}{\alpha^{RT}(a)} = 1 - \frac{\alpha^R}{\alpha^W + \alpha^C + \alpha^R}, \quad z = a, \tag{13b}$$

$$\frac{\alpha_w^{RT}(2a)}{\alpha^{RT}(2a)} = 1 - \frac{[\alpha^{RT}(a)]^2}{\alpha^{RT}(2a)(\alpha^W + \alpha^C + \alpha^R)}, \quad z = 2a, \tag{13c}$$

$$\frac{\alpha_w^{RT}(-a)}{\alpha^{RT}(-a)} = 1 - \frac{\alpha^{RT}(2a)}{\alpha^W + \alpha^C + \alpha^R}, \quad z = -a. \tag{13d}$$

It may be expected that the variation at $z = a$ is greater than that at $z = a/2$, whereas the variation at $z = a/2$ is greater than that at $z = -a$ because $|\alpha^R| > |\alpha^{RT}(a)| > |\alpha^{RT}(2a)|$.

4.3. RESULTS

To turn now to calculated results for the track and wheel presented in section 2, Figure 7 shows the dynamic interaction forces between the wheel and rail for the excitation acting either at mid-span or above a sleeper. The dynamic interaction force is presented in terms of the ratio of the generated force P to the original force F. Two cases are calculated, in which the distance between the excitation point and the wheel–rail interaction point is chosen as 1·8 and 3·6 m respectively. The span length between two sleepers is 0·6 m. The wheel–rail interaction force can be seen to have a similar trend to the transfer receptance of the rail without a wheel on it (see Figure 2) because the interaction force depends upon the transfer receptance according to equation (5). Around 800 Hz the interaction force reaches a high level. The reason for this is that the point receptance sum of the wheel, contact spring and rail, which is the denominator in equation (5), tends to reach its minimum from about 600 Hz, whereas the transfer receptance, the numerator, is relatively large here due to a low decay rate. At high frequencies the wheel–rail interaction force reduces gradually with increasing frequency. Moreover, the interaction forces for distances of 1·8 and 3·6 m are very close to each other above 1200 Hz. This is a consequence of the low decay rate of the wave propagation at high frequencies, which leads to the magnitude of the transfer receptances being similar in each case; see Figure 2.

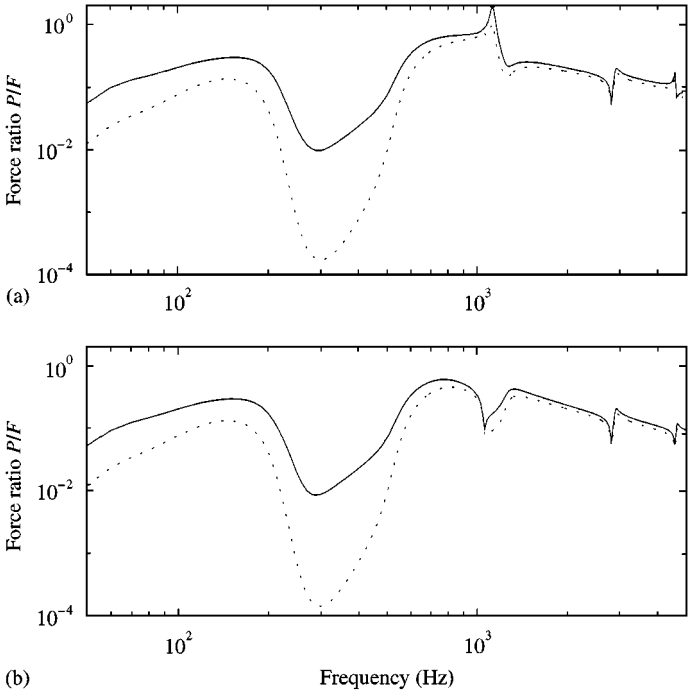

Figure 7. Wheel–rail interaction forces of the discretely supported rail with a single wheel on it: (a) excitation at mid-span, (b) excitation above a sleeper. —— Excitation at 1·8 m from the wheel, ····· excitation at 3·6 m from the wheel.

As the interaction force is related to the rail receptance, the pinned–pinned vibration characteristic can also be recognized in Figure 7. The generated wheel–rail interaction force for the excitation acting at mid-span can be seen even to exceed the original force. This happens at 1100 Hz, just above the first pinned–pinned resonance frequency, where the sum of the point receptances of the wheel, contact spring and rail has a sharp trough; see Figure 5.

Figure 8 shows the point receptances of the rail with and without the additional wheel on it. The point receptance of the rail can be seen to be almost unaffected by the presence of this wheel at low frequencies, as suggested above. At high frequencies, however, it fluctuates around the point receptance of the rail without a wheel–rail interaction. For the 1·8 m distance case the magnitude of the fluctuation is greater than for the 3·6 m distance case. The maximum fluctuation occurs around 700–1000 Hz because the wheel–rail dynamic interaction force reaches a high level around these frequencies; see Figure 7. As the wheel–rail interaction force decreases with increasing frequency at high frequencies, so does the fluctuation of the point receptance.

The pinned–pinned resonance can also be seen clearly in each model for excitation above a sleeper, see Figure 8(b). However, a cancellation of the first pinned–pinned resonance occurs in the case of the excitation acting at mid-span; see Figure 8(a). This can be explained by using equation (9). At the first pinned–pinned resonance, the wavelength is equal to twice the span length and the 1·8 and 3·6 m distances correspond to an integral number of spans. The transfer receptance at the wheel–rail contact point is either in phase or exactly out of phase with the point receptance. On the other hand, the point receptance sum of the wheel, contact spring and rail is approximately equal to the rail point receptance because at the

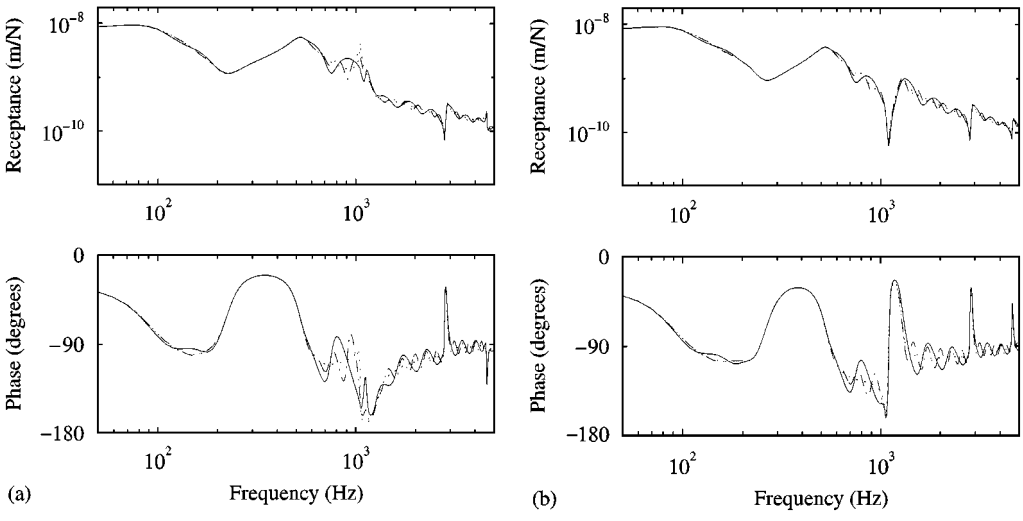

Figure 8. Point receptances of the discretely supported rail with a single wheel on it. (a) excitation at mid-span, (b) excitation above a sleeper. —— For excitation at 1·8 m from the wheel, – · – · – for excitation at 3·6 m from the wheel, ····· for the case without wheel–rail interaction.

pinned–pinned resonance peak it is much higher than both the wheel and the contact spring receptances (Figure 5(a)). For the 1·8 m distance the magnitude of the transfer receptance at this distance is very close to that of the point receptance at the first pinned–pinned resonance so that the second term on the right-hand side in equation (9) is approximately equal to unity. As a result, cancellation of the first pinned–pinned resonance occurs and the receptance of the rail with the wheel present is lower than without it. For the 3·6 m distance the cancellation is reduced because the transfer receptance at 3·6 m is smaller than at 1·8 m. In fact, the cancellation of the first pinned–pinned resonance more or less happens as long as the rail has an additional wheel on it even if it is not at mid-span. This is because at the first pinned–pinned resonance the transfer receptance at the wheel–rail contact point is always approximately in phase or out of phase with the point receptance for most places in a span; the extent of the cancellation depends on the magnitude of the transfer receptance at the wheel–rail contact point.

Figure 9 shows the ratio of the point receptances of the rail with and without the wheel for both 1·8 and 3·6 m distances. The variation in ratio can be seen to be smaller at low frequencies and larger at high frequencies. The largest variation appears near 900 Hz. It reaches about 160% for the 1·8 m distance case and 150% for the 3·6 m distance case. Above 3000 Hz the ratios for both cases are approximately equal although the variation frequencies are different.

5. RAIL VIBRATION BEHAVIOUR WITH MULTIPLE WHEELS

In this section, the rail vibration behaviour is studied taking into account of multiple wheels on it. The model is developed for a discretely supported rail and the receptances at the wheel–rail interaction positions are calculated. Practical consequences are also calculated in terms of the excitation force between the wheel and rail caused by the relative displacement excitation and in terms of the overall vibration energy of the rail, which is related to sound radiation.

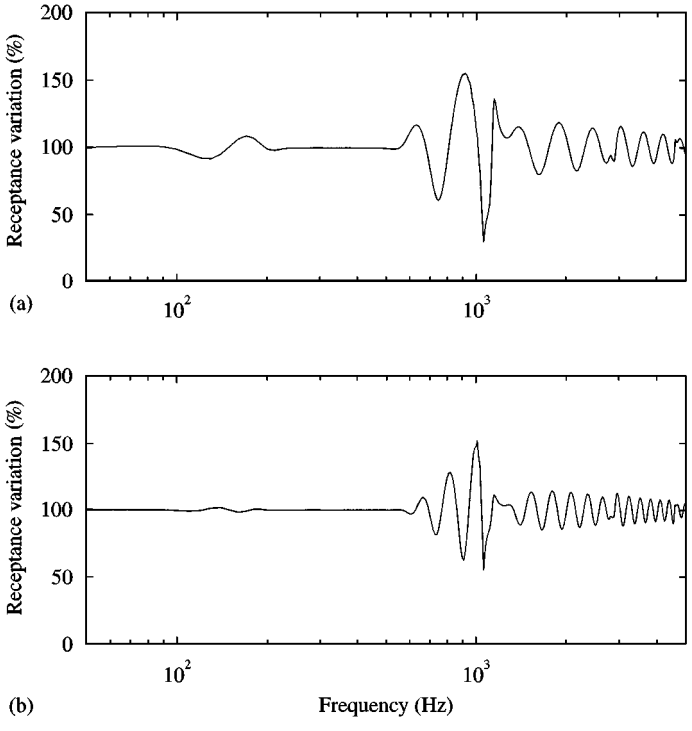

Figure 9. Point receptance ratio of the discretely supported rail with a single wheel on it to the rail without wheel on it. (a) excitation at 1·8 m from the wheel, (b) excitation at 3·6 m from the wheel.

5.1. MODEL FOR THE RECEPTANCES

Figure 10 shows schematically a typical train on a discretely supported rail. As shown in Figure 10 the discretely supported railway track is modelled as an infinite rail with a finite number of discrete supports. This is because the supports at large distances from the point at which the receptance is to be calculated can be neglected due to the wave propagation decay. The number of supports should be chosen large enough to guarantee an acceptable approximate solution. The distances between wheels shown in Figure 10 are chosen to be representative of a bogie container wagon. Owing to the symmetrical arrangement of the wheels, the point receptance need only be calculated at two positions, z_{L1} and z_{L2} or z_{R1} and z_{R2}. To calculate the point receptance at z_{L1} or z_{L2} this wheel should be omitted and a unit force is applied at this position. This point receptance can then be used in equation (1).

In order to calculate the response of the rail, both the discrete supports and the wheels can be replaced by point forces in an extension of the method used in references [9, 12]. The displacement at each wheel–rail contact position (including at z_{L1} and z_{L2}) is a superposition of the response to the unit force at z_{L1} or z_{L2} and of the contributions from the reactions at each wheel–rail contact (excluding z_{L1} or z_{L2}) and at each discrete support. Based on the superposition principle, the responses of the rail at the support points and the wheel–rail contact points to a unit force acting at z_{Li} can be written as

$$u(z_m) = \sum_{\substack{n=1 \\ n \neq Li}}^{M} P_{wn}\alpha^{RT}(z_m, z_n) + \sum_{n=M+1}^{M+N} P_{sn}\alpha^{RT}(z_m, z_n) + \alpha^{RT}(z_m, z_{Li}),\ m = 1, 2, \ldots, M + N, \tag{14}$$

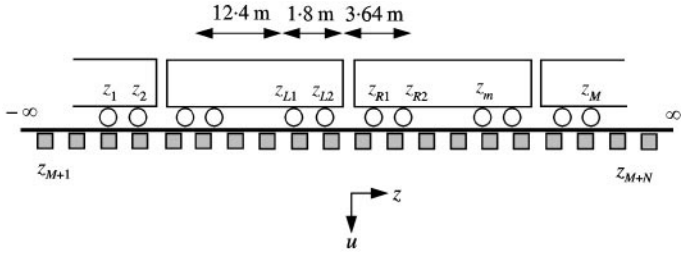

Figure 10. Railway track model with a train (multiple wheels) on the rail. The discrete support is shown only schematically.

where $\alpha^{RT}(z_m, z_n)$ is the transfer receptance of a free rail at z_m with the force acting at z_n, M is the number of wheel–rail interactions under consideration, N is the number of the discrete supports, P_{wn} and P_{sn} are the wheel–rail interaction force and the reaction force of the support respectively and given as

$$P_{wn} = -Z_w u(z_n), \quad n = 1, 2, \ldots, M \text{ and } n \neq L_i, \tag{15}$$

$$P_{sn} = -Z_s u(z_n), \quad n = M+1, M+2, \ldots, M+N, \tag{16}$$

where Z_w is the dynamic stiffness combination of the wheel and contact spring (see sections 3.2 and 3.3),

$$Z_w = \frac{1}{\alpha^W + \alpha^C} = \frac{-K_H K_M M_w \omega^2}{K_H K_M - (K_H + K_M) M_w \omega^2}, \tag{17}$$

and Z_s is the dynamic stiffness of the support [12],

$$Z_s = \frac{K_p(K_b - M_s\omega^2)}{K_p + K_b - M_s\omega^2}. \tag{18}$$

Substituting equations (15) and (16) into equation (14) gives

$$u(z_m) = -\sum_{\substack{n=1 \\ n \neq Li}}^{M} Z_w u(z_n)\alpha^{RT}(z_m, z_n) - \sum_{n=M+1}^{M+N} Z_s u(z_n)\alpha^{RT}(z_m, z_n) + \alpha^{RT}(z_m, z_{Li}),\ m = 1, 2, \ldots, M+N \tag{19}$$

Equation (19) can be solved to give $u(z_m)$ in terms of $\alpha^{RT}(z_m, z_{Li})$ by taking the sum to the left-hand side and then inverting the matrix of coefficients of $u(z_m)$. The displacement at any point on the rail can be obtained by substituting $u(z_m)$ into the equation

$$u(z) = -\sum_{\substack{n=1 \\ n \neq Li}}^{M} Z_w u(z_n)\alpha^{RT}(z, z_n) - \sum_{n=M+1}^{M+N} Z_s u(z_n)\alpha^{RT}(z, z_n) + \alpha^{RT}(z, z_{Li}). \tag{20}$$

Thus, the point receptance at $z = z_{Li}$ and the transfer receptance at z for the rail with multiple wheels on it are given as

$$\alpha_w^R = u(z_{Li}) \quad \text{and} \quad \alpha_w^{RT}(z) = u(z). \tag{21, 22}$$

5.2. RESULTS

Receptances of the discretely supported rail with multiple wheels on it are calculated by using the same parameters as in the previous sections for the track, contact spring and wheels. Figure 11 shows the point receptances. Two cases are calculated. In each case the external excitation acts either at z_{L1} or z_{L2}, which are chosen at mid-span. In one case only the wheel–rail interactions of a pair of bogies (four wheels) at the adjacent ends of two wagons are taken into account. In the other case two more pairs of bogies are added to take account of their wheel–rail interactions (twelve wheels); see Figure 10. From Figure 11 the point receptance at low frequencies can be seen still to be almost equal to that of the rail without a wheel on it due to the high decay rate of the wave propagation in the low frequency region (see Figure 2). Compared to the single wheel–rail interaction case (see Figure 8), however, the fluctuations of the receptance at high frequencies are stronger especially for the excitation acting at z_{L2} because the multiple wheel–rail interactions lead to more wave reflections. An important question is how many wheels should be taken into account when calculating the point receptance of a rail with multiple wheels on it. For the track parameters considered, it is expected that the effect of the wheel–rail interaction for any wheel more than about 10 m away from the point at which the point receptance is calculated may be neglected. This is shown to be the case in Figure 11 as the point receptances from the cases of one and three pairs of bogies on the rail only have very slight differences between them. However, for a track with a softer foundation (lower decay rate) more wheel–rail interactions should be taken into account because the wave propagation decay rate is lower for such a track.

Figure 12 and 13 show the receptances at four wheel–rail contact positions for the external excitation acting at z_{L1} and z_{L2} respectively. Both z_{L1} and z_{L2} are chosen at mid-span or above a sleeper. Calculations are carried out for only four wheel–rail interactions. Since the span length d is chosen as 0·6 m and the distance between two wheels is 1·8 or 3·64 m (see Figure 10) which is exactly or almost exactly equal to an integer times the span length, all the wheels are located at mid-span or above a sleeper when z_{L1} and z_{L2} are at such a position. At high frequencies the pinned–pinned resonances can be

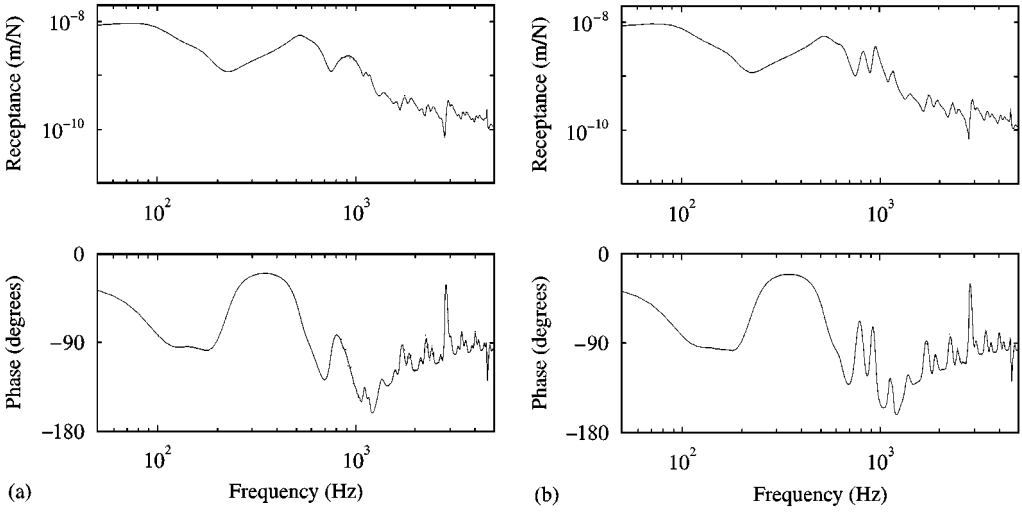

Figure 11. Point receptances of the discretely supported rail with multiple wheels on it: (a) excitation at z_{L1}, (b) excitation at z_{L2}. —— A pair of bogies under consideration, ····· three pairs of bogies under consideration.

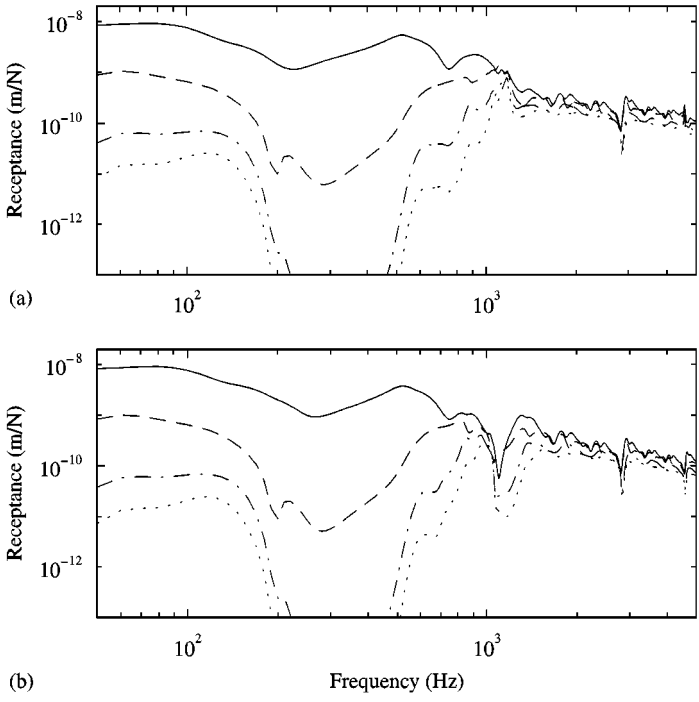

Figure 12. Point and transfer receptances of the discretely supported rail with multiple wheels on it and with excitation at z_{L1}: (a) excitation at mid-span, (b) excitation above a sleeper. —— At z_{L1}, – – – at z_{L2}, –·–·– at z_{R1}, ····· at z_{R2}.

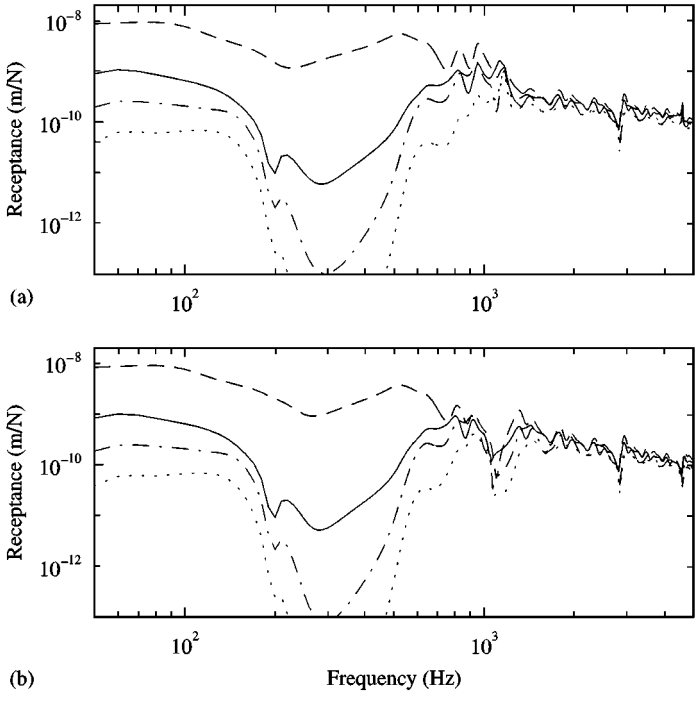

Figure 13. Point and transfer receptances of the discretely supported rail with multiple wheels on it and with excitation at z_{L2}: (a) excitation at mid-span, (b) excitation above a sleeper, key as for Figure 12.

observed. However, the first pinned–pinned resonance peak of the point receptance at mid-span (response at z_{L1} or z_{L2}) is not very noticeable because its cancellation occurs due to the wheel–rail interactions as discussed previously. Because of the low decay rate at high frequencies the receptances at the different positions become closer and closer with increasing frequency, as in Figure 2. Other features are also similar to Figure 2.

5.3. PRACTICAL CONSEQUENCES

The interaction force between the active wheel and the rail caused by the relative displacement excitation can be calculated for the case of multiple wheels on the rail by the formula [2]

$$F = -r/(\alpha^W + \alpha^C + \alpha_w^R), \tag{23}$$

where r is the relative displacement between the wheel and rail and α_w^R is the point receptance of a rail with multiple wheels on it. This is shown in Figure 14. For comparison, the results from the same track but without additional wheel–rail interactions are also given.

Figure 14 shows that at low frequencies the excitation force is virtually unaffected by the presence of multiple wheels on the track. From about 600 Hz, the excitation force for the rail with multiple wheel–rail interactions fluctuates around the curve for the rail without additional wheels on it. The fluctuation mainly appears in the frequency region 700–1200 Hz. The maximum difference in the wheel–rail interaction force reaches about 10 dB at about 1 kHz between the tracks with and without wheels on them. At high frequencies, however, the wheel–rail interaction forces are almost the same for both cases. This is because the receptance of the contact spring is much larger than those of the wheel and rail at high frequencies (see Figure 5), so that the latter can effectively be omitted from the denominator in equation (23).

The rail vibration level due to a unit force excitation is also calculated in terms of the sum of $|v|^2\,\mathrm{d}z$ over a wagon length by considering 12 wheels (three pairs of bogies) on the rail, where $\mathrm{d}z$ is the length of a short piece of rail and v is the vibration velocity of this piece of rail. The results are shown in Figure 15. It can be seen that the rail vibration level due to

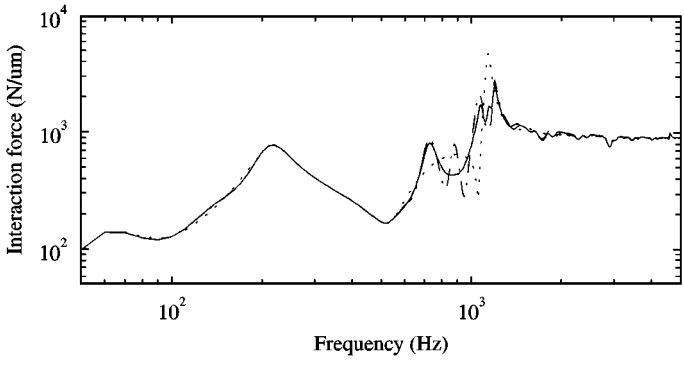

Figure 14. Wheel–rail interaction force due to 1 μm relative displacement excitation. —— from the rail with multiple wheel–rail interactions (three bogies on the rail) and excitation at z_{L1}, – · – · – from the rail with multiple wheel–rail interactions and excitation at z_{L2}, ····· from the rail without additional wheel–rail interactions.

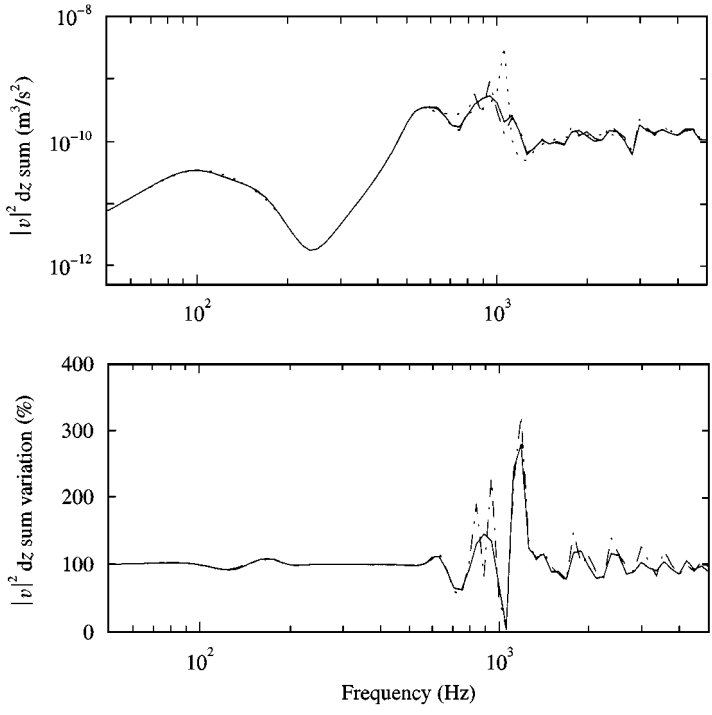

Figure 15. Sum of $|v|^2\,dz$ over a wagon length due to a unit force excitation and its variation ratio relative to the rail without wheels on it, key as for Figure 14.

a unit force excitation for the rail with multiple wheel–rail interactions also shows a similar variation with frequency. Compared with the track without additional wheel–rail interactions, the maximum fluctuation is $\pm$ 2·5 dB, except at the pinned–pinned resonance, where the vibration level for the track without wheels on it exhibits a sharp peak. The reason for the fluctuation at higher frequencies is the presence of the wave reflection from other wheels. At low frequencies, however, the effects of the wave reflection can be ignored because of the high decay rate of the wave propagation. Averaging these results into one-third octave bands does not smooth them completely. Nevertheless, an increase in one band will tend to be compensated by a decrease in adjacent bands and vice versa.

6. CONCLUSIONS

In this paper the effects of the multiple wheel–rail interactions on high frequency rail vibration have been studied. Previous models of noise generation have concentrated on a single wheel interacting with the rail and calculated the track vibration and noise from this situation, under the assumption that the contributions from each wheel/rail interaction can be added incoherently. The paper has addressed the validity of this assumption. For roughness on the wheel it is the correct assumption, but for roughness on the rail more detailed analysis is necessary. It is found that, provided the rail vibration, and noise, is analyzed in frequency bands with a bandwidth of at least 0·8 v/l, where v is the train speed and l is the minimum distance between wheels, the incoherent model gives acceptable results. For typical parameters this corresponds to about 20 Hz. Moreover, when the decay

rate of vibrations in the rail is high, as is the case at low frequencies, the results from the incoherent model are acceptable irrespective of the bandwidth of analysis.

Therefore, for practical analysis it is possible to use the superposition principle and study the rail vibration caused by each wheel in turn. The appropriate application of the superposition principle is to model the rail vibration as a sum of cases in which all wheels are retained in contact with the rail but the roughness of all except one is set to zero. The remaining wheels then become 'passive' dynamic systems attached to the rail. These can introduce reflections in the rail.

In the paper models have been developed to study these effects. Firstly, a simple model of a track with only a single additional wheel on the rail has been developed in order to derive the wheel–rail interaction force and the relationship between the two track models with and without a wheel on it. Based on this simple model and a knowledge of the dynamic behaviour of the wheel and the rail without a wheel on it, the effects of the wheel–rail interaction on the rail vibration have been analyzed in their various aspects for a discretely supported rail. Lastly, a discretely supported track model with multiple wheels on the rail has been developed. The effects of the multiple wheel–rail interactions on rail vibration have been investigated by using this model. Based on this model and the superposition principle, an approach to calculating the track vibration response to multiple wheel–rail excitations is also presented.

The vibration behaviour of the rail with multiple wheels on it is affected by the dynamic properties of both the track and the wheel (including the contact spring). The additional wheel–rail interaction forces are generated according to the wave propagation decay rate in the rail and the point receptance sum of the wheel, contact spring and the rail without wheels on it. If the wave propagation decay rate or the point receptance sum is high, the interaction forces will be small. At low frequencies the wheel–rail interaction forces are small because of the high decay rate of the wave propagation so that the point receptance of the rail is virtually unaffected by the presence of additional wheels. At higher frequencies the point receptance of the rail with wheels on it fluctuates around that of the rail without wheels on it because of the low decay rate of the wave propagation. For the track parameters considered, because of the wave propagation decay, the effect of the wheel–rail interaction may be neglected at distances more than 10 m away. For the track with one or more wheels on it, the first pinned–pinned resonance is observed to experience cancellation when an excitation acts at mid-span. Moreover, in this case the generated wheel–rail interaction force is expected to exceed the original excitation at a frequency slightly above the first pinned–pinned resonance.

By using the point receptance of the rail with multiple wheels on it and the relative displacement excitation model, a more realistic estimate of the wheel–rail interaction force can be achieved than if only a single wheel is considered. Then the mean-square response of the track to each wheel can be added by treating each active wheel–rail interaction as an uncorrelated source. Based on this approach, the wheel and rail vibration may be expected to be predicted more accurately, as the wheel–rail rolling noise may be.

REFERENCES

1. P. J. REMINGTON 1987 *Journal of the Acoustical Society of America* **81**, 1805–1823. Wheel/rail rolling noise I: theoretical analysis.
2. S. L. GRASSIE, R. W. GREGORY, D. HARRISON and K. L. JOHNSON 1982 *Journal of Mechanical Engineering Science* **24**, 77–90. The dynamic response of railway track to high frequency vertical excitation.

3. D. J. THOMPSON 1993 *Journal of Sound and Vibration* **161**, 387–400. Wheel–rail noise generation, Part I: introduction and interaction model.
4. K. L. KNOTHE and S. L. GRASSIE 1993 *Vehicle System Dynamics* **22**, 209–262. Modelling of railway track and vehicle/track interaction at high frequencies.
5. M. A. HECKL 1991 *Report to the ORE Committee* C163. Acoustic behaviour of a periodically supported Timoshenko beam.
6. D. J. THOMPSON 1993 *Journal of Sound and Vibration* **161**, 421–446. Wheel–rail noise generation, Part III: rail vibration.
7. B. RIPKE and K. KNOTHE 1991 *Fortschritt-Berichte VDI Reihe* 11 No. 155. Die unendlich lange Schiene auf diskreten Schwellen bei harmonischer Einzellasterregung.
8. L. GRY 1996 *Journal of Sound and Vibration* **195**, 477–505. Dynamic modelling of railway track based on wave propagation.
9. T. X. WU and D. J. THOMPSON 1999 *Journal of Sound and Vibration* **224**, 329–348. A double Timoshenko beam model for vertical vibration analysis of railway track at high frequencies.
10. T. X. WU and D. J. THOMPSON 1999 *Journal of the Acoustical Society of America* **106**, 1369–1376. Analysis of lateral vibration behaviour of railway track at high frequencies using a continuously supported multiple beam model.
11. M. A. HECKL 1995 *Acustica* **81**, 559–564. Railway noise—can random sleeper spacing help?
12. T. X. WU and D. J. THOMPSON 1999 *Journal of Sound and Vibration* **219**, 881–904. The effects of local preload on the foundation stiffness and vertical vibration of railway track.
13. D. J. THOMPSON 1990 *Ph.D. thesis, University of Southampton.* Wheel–rail noise: theoretical modelling of the generation of vibrations.
14. A. IGELAND 1996 *Proceedings of the Institution of Mechanical Engineers.* Part *F* **210**, 11–20. Railhead corrugation growth explained by dynamic interaction between track and bogie wheelsets.
15. N. VINCENT and D. J. THOMPSON 1995 *Vehicle System Dynamics* Supplement **24**, 100–114. Track dynamic behaviour at high frequencies. Part 2: experimental results and comparisons with theory.
16. D. J. THOMPSON 1993 *Journal of Sound and Vibration* **161**, 401–419. Wheel–rail noise generation, Part II: wheel vibration.
17. L. MEIROVITCH 1986 *Elements of Vibration Analysis*, see page 75. New York: McGraw-Hill, second edition.
18. D. E. NEWLAND 1984 *An Introduction to Random vibrations and Spectral Analysis.* London: Longman, second edition.

APPENDIX A. APPLICATION OF THE PRINCIPLE OF SUPERPOSITION TO RELATIVE DISPLACEMENT INPUTS

A.1. PRINCIPLE OF SUPERPOSITION

The principle of superposition states that 'for linear systems the responses to a given number of distinct excitations can be obtained separately and then combined to obtain the aggregate response' [17]. The usual application of this in structural vibration analysis is for the case of two forces applied to a structure. If these two forces are $\{F_1, F_2\}$, applied at points 1 and 2, the total response is the sum of the response to $\{F_1, 0\}$ and the response to $\{0, F_2\}$. For a particular frequency, this total response can be written in terms of mobilities,

$$v_i = Y_{i1}F_1 + Y_{i2}F_2, \tag{A1}$$

where Y_{ij} is the velocity at point i to a unit force at point j and v_i is the total velocity of point i. (For non-harmonic solutions, the superposition principle further allows the solutions at different frequencies to be added.) For the special case where point i is either of the excitation points, equation (A1) can be written using a matrix of mobilities, in this case 2×2:

$$\begin{Bmatrix} v_1 \\ v_2 \end{Bmatrix} = \begin{bmatrix} Y_{11} & Y_{12} \\ Y_{21} & Y_{22} \end{bmatrix} \begin{Bmatrix} F_1 \\ F_2 \end{Bmatrix}. \tag{A2}$$

For this case the superposition principle in effect says

$$\begin{Bmatrix} v_1 \\ v_2 \end{Bmatrix} = \begin{bmatrix} Y_{11} & Y_{12} \\ Y_{21} & Y_{22} \end{bmatrix} \begin{Bmatrix} F_1 \\ 0 \end{Bmatrix} + \begin{bmatrix} Y_{11} & Y_{12} \\ Y_{21} & Y_{22} \end{bmatrix} \begin{Bmatrix} 0 \\ F_2 \end{Bmatrix}. \tag{A3}$$

However if the system inputs are *velocities*, the forces generated at the input points are the outputs. These are given by

$$\begin{Bmatrix} F_1 \\ F_2 \end{Bmatrix} = \begin{bmatrix} Z_{11} & Z_{12} \\ Z_{21} & Z_{22} \end{bmatrix} \begin{Bmatrix} v_1 \\ v_2 \end{Bmatrix}, \tag{A4}$$

where the matrix $[Z] = [Y]^{-1}$ is the impedance matrix. In general, for a matrix of dimension two or more, $Z_{ij} \neq 1/Y_{ij}$. Equation (A4) is also an expression of the superposition principle, but in this case the two situations being superposed have a *velocity* imposed at one of the excitation points: i.e.,

$$\begin{Bmatrix} F_1 \\ F_2 \end{Bmatrix} = \begin{bmatrix} Z_{11} & Z_{12} \\ Z_{21} & Z_{22} \end{bmatrix} \begin{Bmatrix} v_1 \\ 0 \end{Bmatrix} + \begin{bmatrix} Z_{11} & Z_{12} \\ Z_{21} & Z_{22} \end{bmatrix} \begin{Bmatrix} 0 \\ v_2 \end{Bmatrix}. \tag{A5}$$

Thus, the first of the two situations being superposed is represented by

$$\begin{Bmatrix} F_1 \\ F_2 \end{Bmatrix}_1 = \begin{bmatrix} Z_{11} & Z_{12} \\ Z_{21} & Z_{22} \end{bmatrix} \begin{Bmatrix} v_1 \\ 0 \end{Bmatrix}. \tag{A6}$$

In this equation, point 1 is excited by a velocity v_1, while point 2 is clamped (i.e., its velocity is set to 0), not free as in the form represented by equation (A3). Conversely, it can be seen that here both forces are non-zero, F_2 being the reaction force required to constrain the velocity v_2 to 0.

In the paper, the equations of wheel/rail interaction are expressed in a form equivalent to equation (A4), with the roughness forming a relative velocity (or displacement) excitation. Although the excitation is a *relative* velocity rather than an externally applied absolute velocity, if one writes out the equations for multiple wheels on a rail, one arrives at an equation resembling (A4). This is done in the following section.

A.2. ESTABLISHING THE SUPERPOSITION PRINCIPLE FOR RELATIVE DISPLACEMENT INPUTS

Consider a track with two wheels on it, as in Figure 1(a) of the paper, and with single frequency roughness excitations, r_1 at wheel 1 and r_2 at wheel 2. As a result of these roughnesses, interaction forces are generated at each wheel/rail contact. Only the vertical direction is considered. For of the sake of consistency with the paper, receptances are used rather than mobilities and displacements rather than velocities.

Write the total interaction forces at points 1 and 2 as F_{t1} and F_{t2} (positive downwards on the rail). The vibration amplitudes of the wheel are written as x_1^W and x_2^W and those of the rail as x_1^R and x_2^R (all positive downwards). Define the rail dynamic properties by the 2×2 matrix of receptances $[\alpha_{ij}^R]$ and the wheels (which may be taken to include the contact springs) by the two individual receptances α_i^W. This ignores any coupling through the vehicle which would introduce terms of the form α_{ij}^W. Then the equations of motion for the wheels are

$$\alpha_i^W F_{ti} = -x_i^W, \tag{A7}$$

while for the track

$$[\alpha_{ij}^R]\{F_{ij}\} = \{x_i^R\}. \tag{A8}$$

Continuity of displacement at the contact points gives

$$x_i^R - x_i^W = r_i. \tag{A9}$$

These equations can be rearranged to give

$$([\alpha_{ij}^R] + [\alpha_{ij}^W])\{F_{tj}\} = \{r_i\}. \tag{A10}$$

Since the roughnesses r_i are the system inputs, this equation can be inverted to give the contact forces in terms of the roughnesses:

$$\{F_{tj}\} = ([\alpha_{ij}^R] + [\alpha_{ij}^W])^{-1}\{r_i\}. \tag{A11}$$

This equation resembles equation (A4) above. It is this equation to which the superposition principle is applied in pictorial form in Figure 1 of the paper:

$$\begin{Bmatrix} F_{t1} \\ F_{t2} \end{Bmatrix} = \begin{Bmatrix} F_1 \\ P_2 \end{Bmatrix} + \begin{Bmatrix} P_1 \\ F_2 \end{Bmatrix}, \tag{A12}$$

with

$$\begin{Bmatrix} F_1 \\ P_2 \end{Bmatrix} = ([\alpha_{ij}^R] + [\alpha_{ij}^W])^{-1} \begin{Bmatrix} r_1 \\ 0 \end{Bmatrix}, \tag{A13a}$$

$$\begin{Bmatrix} P_1 \\ F_2 \end{Bmatrix} = ([\alpha_{ij}^R] + [\alpha_{ij}^W])^{-1} \begin{Bmatrix} 0 \\ r_2 \end{Bmatrix}, \tag{A13b}$$

where the symbol F is used for the force acting at the contact point where roughness is present and P is used for the other contact point. The response of the wheel or rail to these forces can be calculated from equations (A7) and (A8) above.

Equations (A12, 13) establish the principle upon which the model is based, as illustrated in Figure 1 of the paper. Thus, the response of the system can be calculated by setting all of the roughnesses to zero except one whilst retaining contact between all the wheels and the track. The response to roughness excitation at each wheel can thereby be calculated in turn and combined by an appropriate superposition.

From equation (A8) the response of the rail at points 1 and 2 due only to the roughness r_1 at point 1 is

$$\begin{Bmatrix} x_1^R \\ x_2^R \end{Bmatrix} = \begin{bmatrix} \alpha_{11}^R & \alpha_{12}^R \\ \alpha_{21}^R & \alpha_{22}^R \end{bmatrix} \begin{Bmatrix} F_1 \\ P_2 \end{Bmatrix}. \tag{A14}$$

Combining this with equation (A13a), one has

$$\begin{Bmatrix} x_1^R \\ x_2^R \end{Bmatrix} = \begin{bmatrix} \alpha_{11}^R & \alpha_{12}^R \\ \alpha_{21}^R & \alpha_{22}^R \end{bmatrix} ([\alpha_{ij}^R] + [\alpha_{ij}^W])^{-1} \begin{Bmatrix} r_1 \\ 0 \end{Bmatrix}, \tag{A15}$$

This appears at first sight to differ from the form used in the paper. However, it can be rearranged in terms of the receptance of wheel 1 and the receptance of the *track with wheel* 2 *attached to it*, i.e., as in Figure 1(b) of the paper. The equivalence of this to equation (A15) can also be proved mathematically as follows.

A.3. EXPRESSION IN TERMS OF RAIL RECEPTANCE WITH ADDITIONAL WHEEL ON IT

Expanding the matrix inverse in equation (A15) gives

$$([\alpha_{ij}^R] + [\alpha_{ij}^W])^{-1} = \begin{bmatrix} \alpha_{11}^R + \alpha_1^W & \alpha_{12}^R \\ \alpha_{21}^R & \alpha_{22}^R + \alpha_2^W \end{bmatrix}^{-1}$$

$$= \frac{1}{(\alpha_{11}^R + \alpha_1^W)(\alpha_{22}^R + \alpha_2^W) - \alpha_{12}^R \alpha_{21}^R} \begin{bmatrix} \alpha_{22}^R + \alpha_2^W & -\alpha_{12}^R \\ -\alpha_{21}^R & \alpha_{11}^R + \alpha_1^W \end{bmatrix}. \tag{A16}$$

Hence upon extracting just x_1^R from equation (A15)

$$\frac{x_1^R}{r_1} = \frac{\alpha_{11}^R(\alpha_{22}^R + \alpha_2^W) - \alpha_{12}^R \alpha_{21}^R}{(\alpha_{11}^R + \alpha_1^W)(\alpha_{22}^R + \alpha_2^W) - \alpha_{12}^R \alpha_{21}^R}. \tag{A17}$$

Upon writing this in the form

$$\frac{r_1}{x_1^R} = \frac{(\alpha_{11}^R + \alpha_1^W)(\alpha_{22}^R + \alpha_2^W) - \alpha_{12}^R \alpha_{21}^R}{\alpha_{11}^R(\alpha_{22}^R + \alpha_2^W) - \alpha_{12}^R \alpha_{21}^R} = 1 + \frac{\alpha_1^W(\alpha_{22}^R + \alpha_2^W)}{\alpha_{11}^R(\alpha_{22}^R + \alpha_2^W) - \alpha_{12}^R \alpha_{21}^R}. \tag{A18}$$

and defining the term α_1^{RW} as

$$\alpha_1^{RW} = \frac{\alpha_{11}^R(\alpha_{22}^R + \alpha_2^W) - \alpha_{12}^R \alpha_{21}^R}{(\alpha_{22}^R + \alpha_2^W)} = \alpha_{11}^R - \frac{\alpha_{12}^R \alpha_{21}^R}{(\alpha_{22}^R + \alpha_2^W)}, \tag{A19}$$

this can be recognized as the receptance of a rail with an additional wheel on it, as given by equation (8) in the paper. This allows equation (A18) to be written simply as

$$\frac{r_1}{x_1^R} = 1 + \frac{\alpha_1^W}{\alpha_1^{RW}}, \tag{A20}$$

which can be rearranged into the form

$$\frac{x_1^R}{r_1} = \frac{\alpha_1^{RW}}{\alpha_1^{RW} + \alpha_1^W}. \tag{A21}$$

This is the relative displacement excitation equation for a single wheel/rail contact, equivalent to equation (1) of the paper (apart from the omission of the contact receptance which has been included into α^W here), but with the rail receptance α^R replaced by α_1^{RW}. This is the method used in the paper.

Hence, it has been shown that the model of a relative displacement excitation at a single wheel can be applied to a case with multiple wheels by first considering the roughness at each wheel/rail contact point separately, and then using the model with the rail receptance modified to include the additional (passive) wheels. The above can, in principle, also be extended to the case of more than two wheels on the rail although the formulation is much more complicated and no further insight would be gained.

APPENDIX B. CORRELATION BETWEEN MULTIPLE WHEEL-RAIL EXCITATIONS

B.1. PROBLEM

Suppose that a track is excited by two forces F_1 and F_2 at a distance l apart. These forces are both assumed to be the result of the same ergodic stationary random process with spectral density $S_F(\omega)$. Suppose that the forces are identical apart from a time lag $t_0 = l/v$ corresponding to the train speed v. The forces acting are thus $F_1 = F(t)$ and $F_2 = F(t - t_0)$.

For a harmonic force at frequency ω, the vibration response at some position z on the rail is given by

$$u(z, t) = \alpha^{RT}(z, 0)F(t) + \alpha^{RT}(z, l)F(t - t_0), \tag{B1}$$

where $\alpha^{RT}(z_1, z_2)$ is the transfer receptance of the rail at frequency ω giving the response at z_1 due to a unit force at z_2. Write $H_1(\omega) = \alpha^{RT}(z, 0)$, $H_2(\omega) = \alpha^{RT}(z, l)$. Then for a system with two inputs and one output [18], the spectral density of the response $u(z, t)$ due to two random forces F_1 and F_2 is

$$S_{u(z)}(\omega) = |H_1(\omega)|^2 S_{F_1}(\omega) + |H_2(\omega)|^2 S_{F_2}(\omega) + H_1^*(\omega)H_2(\omega)S_{F_1F_2}(\omega) + H_2^*(\omega)H_1(\omega)S_{F_2F_1}(\omega). \tag{B2}$$

This can be simplified by noting that the auto-spectral densities, $S_{F_1}(\omega) = S_{F_2}(\omega) = S_F(\omega)$. The cross-spectral densities between F_1 and F_2 can be found from the definition in terms of the cross-correlation function

$$\mathrm{S}_{F_1F_2}(\omega) = \frac{1}{2\pi}\int_{-\infty}^{\infty} R_{F_1F_2}(\tau)\,\mathrm{e}^{-\mathrm{i}\omega\tau}\,\mathrm{d}\tau, \tag{B3}$$

with

$$R_{F_1F_2}(\tau) = \lim_{T\to\infty}\frac{1}{2T}\int_{-T}^{T} F_1(t)\,F_2(t + \tau)\,\mathrm{d}t. \tag{B4}$$

Substituting for F_1 and F_2 yields

$$R_{F_1F_2}(\tau) = \lim_{T\to\infty}\frac{1}{2T}\int_{-T}^{T} F(t)\,F(t - t_0 + \tau)\,\mathrm{d}t = R_F(\tau - t_0). \tag{B5}$$

So

$$\mathrm{S}_{F_1F_2}(\omega) = \frac{1}{2\pi}\int_{-\infty}^{\infty} R_F(\tau - t_0)\mathrm{e}^{-\mathrm{i}\omega\tau}\,\mathrm{d}\tau = \frac{\mathrm{e}^{-\mathrm{i}\omega t_0}}{2\pi}\int_{-\infty}^{\infty} R_F(\tau)\mathrm{e}^{-\mathrm{i}\omega\tau}\,\mathrm{d}\tau = \mathrm{e}^{-\mathrm{i}\omega t_0}S_F(\omega). \tag{B6}$$

Similarly

$$S_{F_2F_1}(\omega) = \mathrm{e}^{\mathrm{i}\omega t_0}S_F(\omega). \tag{B7}$$

Substituting into equation (B2) gives

$$S_{u(z)}(\omega) = \{|H_1(\omega)|^2 + |H_2(\omega)|^2 + 2\,\mathrm{Re}(H_1^*(\omega)H_2(\omega)\mathrm{e}^{-\mathrm{i}\omega t_0})\}S_F(\omega). \tag{B8}$$

Write $H_2(\omega)/H_1(\omega) = \alpha^{RT}(z, l)/\alpha^{RT}(z, 0) = A(\omega)\mathrm{e}^{\mathrm{i}\phi(\omega)}$, where $A(\omega)$ is the frequency-dependent amplitude ratio and $\phi(\omega)$ is the phase difference in the transfer receptances. Inserting this

into equation (B8) gives the spectral density of the response for coherent forces:

$$S_{u(z),coh}(\omega) = |\alpha^{RT}(z,0)|^2 (1 + A^2 + 2A\cos(\omega t_0 - \phi)) S_F(\omega). \tag{B9}$$

This can be compared with the spectral density of the response at z to two incoherent forces of identical spectral density, $S_F(\omega)$:

$$S_{u(z),incoh}(\omega) = |\alpha^{RT}(z,0)|^2 (1 + A^2) S_F(\omega). \tag{B10}$$

Thus, the effect of the interrelation of the two forces F_1 and F_2 can be given by the ratio of equations (B9) and (B10):

$$\Gamma(\omega) = \frac{S_{u(z),coh}(\omega)}{S_{u(z),incoh}(\omega)} = \frac{(1 + A^2 + 2A\cos(\omega t_0 - \phi))}{1 + A^2} = 1 + \frac{2A\cos(\omega t_0 - \phi)}{1 + A^2}. \tag{B11}$$

The function Γ oscillates about 1, with its maxima and minima occurring at frequencies $\omega = (n\pi + \phi)/t_0$ for integer values of n. When $A = 1$, the function Γ oscillates between 0 and 2, otherwise the magnitude of the oscillations, $2A/(1 + A^2)$ is less than 1.

B.2. FREQUENCY BAND AVERAGE

The track response to a passing train is a transient phenomenon, and is usually required in terms of frequency band averages, for example in one-third octave bands or constant bandwidth bands. For a frequency band with lower frequency ω_L and upper frequency ω_U, the mean-square response is

$$S_u^b(\omega_c) = 2\int_{\omega_L}^{\omega_U} S_u(\omega)\,\mathrm{d}\omega, \tag{B12}$$

where b indicates a band average. The centre frequency of the band is here defined as $\omega_c = (\omega_U + \omega_L)/2$. The factor 2 in equation (B12) comes from the conversion from two- to one-sided spectra. Upon assuming that neither the spectral density of the force nor the receptance vary strongly within the band,

$$S_{u,coh}^b(\omega_c) \approx |\alpha^{RT,b}(z,0)|^2 \left((1 + A^2)(\omega_U - \omega_L) + \frac{2A}{t_0}(\sin(\omega_U t_0 - \phi) - \sin(\omega_L t_0 - \phi)) \right) S_F^b(\omega_c)$$

$$= |\alpha^{RT,b}(z,0)|^2 \left((1 + A^2)(\omega_U - \omega_L) + \frac{4A}{t_0}\cos(\omega_c t_0 - \phi)\sin(\delta\omega t_0) \right) S_F^b(\omega_c), \tag{B13}$$

where $\delta\omega = (\omega_U - \omega_L)/2$ is half the bandwidth of the band. The equivalent expression for two incoherent forces, from equation (B10) is

$$S_{u,incoh}^b(\omega_c) = |\alpha^{RT,b}(z,0)|^2 (1 + A^2)(\omega_U - \omega_L) S_F^b(\omega_c). \tag{B14}$$

The ratio of these two results gives a band-averaged equivalent to the function Γ:

$$\Gamma^b(\omega_c) = \frac{S_{u,coh}^b(\omega_c)}{S_{u,incoh}^b(\omega_c)} = 1 + \frac{2A\cos(\omega_c t_0 - \phi)}{(1 + A^2)} \left(\frac{\sin(\delta\omega t_0)}{\delta\omega t_0} \right). \tag{B15}$$

As in equation (B11), this contains an oscillatory part which varies with frequency, its maxima and minima occurring at the frequencies $\omega_c = (n\pi + \phi)/t_0$ for integer values of n,

and its amplitude decreasing as A differs from 1. However, the integration over a frequency band has introduced the additional term which depends on $\delta\omega t_0$, the product of half the bandwidth and the time lag between the two forces. The greater the bandwidth, the smaller the magnitude of the oscillatory term in equation (B15). For $\delta\omega\, t_0 > 2{\cdot}5$, the oscillatory term is less than 0·25, or $\pm$ 1 dB. This occurs for frequency bands with bandwidth greater than $0{\cdot}8/t_0$.

B.3. RESULTS AND DISCUSSION

Some typical values can be used to demonstrate the nature of these results. The minimum distance between two wheels, l, is about 1·8 m for two wheels in a common bogie. For a train speed of 160 km/h, this gives $t_0 = 0{\cdot}04$ s. This yields $\delta\omega t_0 > 2{\cdot}5$ if the bandwidth of the band is at least 20 Hz. For one-third octave bands, this condition is satisfied for the frequency bands above 80 Hz.

Although the receptances α^{RT} depend on the details of the track and on the location z, the propagation of vibration waves along a track can be expressed in terms of a structural wavenumber, k, and a decay rate Δ in dB/m [6, 15]. The wavenumber determines the relative phase of the response along the track. The decay rate is related to the exponential decay of vibration amplitude, $|u(z)| \sim \mathrm{e}^{-\beta z}$ where $\beta = \Delta/8{\cdot}686$. Thus for $z \leqslant 0$, the amplitude ratio $A \approx \mathrm{e}^{-\beta l}$, for $0 \leqslant z \leqslant l$, $A \approx \mathrm{e}^{-\beta(l-2z)}$, and for $z \geqslant l$, $A \approx \mathrm{e}^{\beta l}$.

Typically, for vertical bending, waves do not propagate freely at low frequencies, and the decay rate is around 10 dB/m for frequencies up to 200–400 Hz, this frequency depending on the pad stiffness. Above this frequency, wave propagation occurs and the decay rate drops, typically to around 1 dB/m [15]. A decay rate of 10 dB/m corresponds to a factor $A \approx \mathrm{e}^{-\beta l}$ of 0·13, and a factor of $2A/(1 + A^2)$ of 0·25. Thus for the region $z \leqslant 0$ or $z \geqslant l$, the largest variation expected is $\pm$ 1 dB. At $z = l/2$, however, $A = 1$ whatever the decay rate.

Figure B1 shows the function Γ^b calculated for the above parameters, for the cases of 0 and 10 dB/m and ignoring the phase change along the rail, ϕ. Including the phase differences would only affect the position of the maxima and minima not their magnitudes. The case with non-zero decay rate corresponds only to the situations $z \leqslant 0$ or $z \geqslant l$. Results are given for one-third octave bands. From this figure it can be seen that the effect of including the correlation between the forces at the two wheels is only significant below 200 Hz, and then only for the case where the decay rate is set to zero. It is in any case less than 1 dB for all frequency bands above 80 Hz. Since on practical tracks the decay rate at frequencies below 200 Hz is around 10 dB/m, the effect of interference between the excitation due to multiple wheels is expected to be, at most, $\pm$ 1 dB even for lower frequency bands. In the region above 200 Hz it is less than $\pm$ 0·2 dB even when the decay rate is set to 0.

Figure B2 shows equivalent results for 1/12 octave bands. Here the oscillation is greater with no decay included in the track response, but with the decay in the track it is again limited to about $\pm$ 1 dB.

It has thus been shown that the interference effects of two coherent forces on the rail with a time lag t_0 between them is limited, provided either that the bandwidth of analysis is at least $0{\cdot}8/t_0$ or that the decay rate is high. Either or both these conditions apply in most typical situations. The exception is between two wheels of the same bogie where, at low frequencies (or in narrow frequency bands), the level can oscillate between a level 3 dB higher than the result of the incoherent sum and zero. However this point, mid-way between two wheels, corresponds to a spatial minimum in the response and does not contribute significantly to the spatially averaged response at low frequencies.

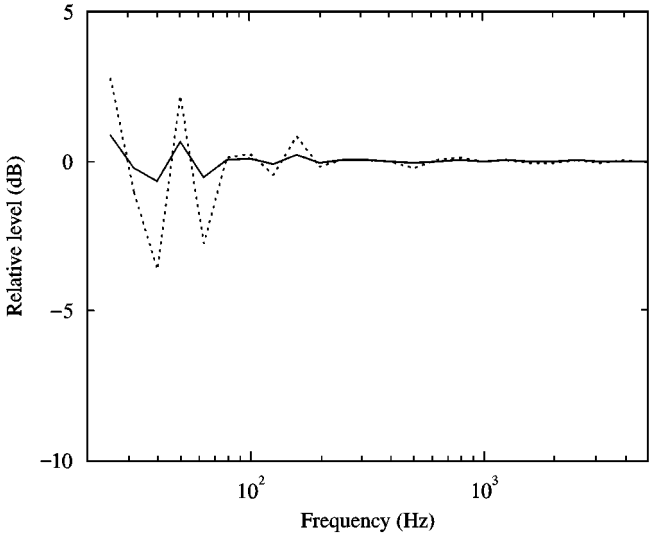

Figure B1. Effect of including coherent excitation at two wheels compared to including them as incoherent excitation for 1/3 octave responses. —— with decay rate 10 dB/m, ····· with no decay of the rail vibration.

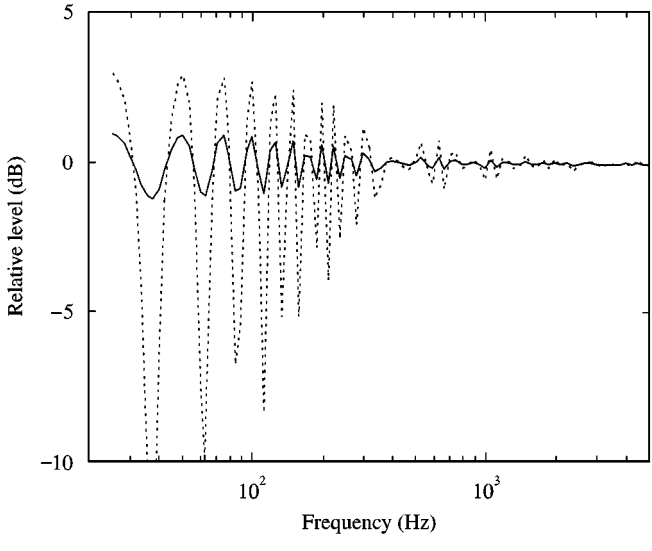

Figure B2. As Figure B1 but for 1/12 octave bands.